Electronic structure in space-charge layers of narrow-gap semiconductors in the presence of strong magnetic fields

Saadi Lamari
Institut de Physique, Université Ferhat Abbas, Setif 19000, Algeria
(Received 1 March 1999)

In the presence of strong normal magnetic fields, the electronic structure of inversion electrons in the space-charge layers of narrow-gap semiconductors is considered. We use the effective mass and local-density approximations and include band mixing exactly in the full eight-band Kane model. The wave function satisfies special derived boundary conditions which are generalized to include the split-off band; moreover, an improved semiclassical approximation is introduced and successfully exploited to deduce the subband structure. A special unitary transformation taking the finite field problem into its zero-field counterpart is found. In addition, the same transformation allows for the separation of the two contributions to the spin splitting of the energy levels: The one due to the self-consistent field and the one due to the external normal magnetic field. Extensive numerical computations are carried out on InSb metal oxide semiconductor field-effect transistors and used to interpret existing experimental cyclotron resonance data. The cyclotron masses of the levels involved in cyclotron resonance are computed as a function of areal electron density $N_{\rm inv}$ and compared to experiment with which they show satisfactory agreement. In the ground subband, our theory predicts multiple masses not found in previous interpretations; moreover, the Fermi energy $E_F(B)$ oscillates around $E_F(B=0)$ as $N_{\rm inv}$ varies leading to an effective mass m^* showing the same behavior through a combination of nonparabolicity, Landau-level filling, and the Pauli exclusion principle. [S0163-1829(99)01340-5]

I. INTRODUCTION

Narrow-gap semiconductors (NGS) such as InSb and $Hg_{1-x}Cd_xTe$ alloys have a fairly complex band structure[1] from which follows a vast variety of exciting optical and magneto-optical properties.[2] These peculiarities make them excellent candidates for fundamental research as well as technological applications in areas such as infrared (IR) detection.[3] Substantial studies have been carried out, on different systems based on these materials in many different experimental settings. Among these investigations, a very large number have been devoted to studies of the electronic properties of inversion layers encountered[4] in MOSFETs (metal oxide semiconductor field-effect transistors). In these systems, a *p*-type semiconductor substrate is covered with a thin insulating layer, usually an oxide, which is itself covered with a metallic layer called the ''gate.'' When the gate voltage V_g exceeds a threshold value $V_t>0$, a thin quasi-two-dimensional (2D) electron gas, called an inversion layer, forms and is trapped between the insulating interface and the depleted substrate region.[5] The motion normal to the interface becomes quantized, the electrons in the inversion layer occupy so-called 2D subbands, and the system thus formed acquires many properties of its own.

Inversion layers on NGS are special in many respects. First, their bulk conduction-band dispersion is not parabolic and is rather ''relativisticlike.''[6] Second, their very small band-edge mass m^* translates into a small density of state $D(E)$ which in turn leads to the occupation of a large number of subbands for a given areal electronic density $N_{\rm inv}$. Third, the electron wave function in these materials is not a scalar but transforms rather as an eight-component spinor. This particularity imposes on the wave function special boundary conditions (BC) at the insulator/semiconductor interface.[7,8] Moreover, in the presence of a strong magnetic field, the Landau spacing of the levels is comparable to the intersubband spacing. These important peculiarities make the interpretation of experiments delicate and the need for theoretical self-consistent calculations a necessity.[9]

Among the published theoretical works[7,10] on NGS inversion layers a large share deals with the system in zero magnetic field. Some others, however, include the effects of a finite magnetic field in a simplified two-band model[11] and, in addition to that, assume the system to be in the quantum limit where only one subband is occupied. On the other hand, Shubnikov–de Hass, (SdH) measurements[4] indicate the occupation of many more subbands, typically up to four (eight if we include spin), in commonly encountered situations. In the same work,[4] cyclotron resonance experiments are reported and their authors stress in their interpretation the occupation of many subbands to get a best fit. The results of the simplified theoretical model already alluded to cannot be directly compared to experiment and the need for a theory where the experimental conditions are taken into account is obvious. The problem has recently been addressed by the present author in a short publication[9] in which the important details of the theory were not exposed. Because of the relation of this problem to systems such as CdTe/InSb heterojunctions,[12] NGS quantum wires,[13] etc., we deem it useful to give a full account of the theory underlying the results already published.

The paper is organized as follows: In Sec. II we give a full presentation of the zero-field theory and explicitly expose the basic equations for three particular models. Consequently, our self-consistent results are shown and compared to experiment. In Sec. III we use the self-consistent potential of Sec. II and develop a theory for the finite *B* field case. The

basic equations are derived and a method for their solution is systematically shown and applied; the results are then compared to experiment. Section IV concludes the paper and summarizes the salient features of this work and its possible applications. In addition, the paper contains two appendixes *A* and *B* which further complete the expositions in Secs. II and III, respectively.

II. ZERO-FIELD THEORY

A. Formulation of the problem

This section presents the general theory used to find the electronic structure in the inversion layer in the absence of a magnetic field. For convenience we suppose the semiconductor to be on the right-hand side and the insulator on the left-hand side. Let the *x* axis be normal to the interface which is taken to lie in the *yz* plane. We work in the full eight-band Kane model and denote by $|1\rangle,|2\rangle,...,|8\rangle$ the basis vectors in terms of which we expand the wave function $|\psi\rangle$ within the $\mathbf{k}\cdot\mathbf{p}$ approximation. For the sake of clarity the expressions for the basis vectors and the $\mathbf{k}\cdot\mathbf{p}$ Hamiltonian are given in Appendix A. Let $H(\mathbf{K})$, with $\mathbf{K}=k_x\hat{\mathbf{e}}_1+k_y\hat{\mathbf{e}}_2+k_z\hat{\mathbf{e}}_3$, denote the Kane $\mathbf{k}\cdot\mathbf{p}$ Hamiltonian in which all the quadratic *k* terms are neglected. This approximation for the full Hamiltonian is valid only when dealing with electrons in the lowest Γ_6 conduction band and is widely used; in the expression for $\mathbf{K}$, $\hat{\mathbf{e}}_1$, $\hat{\mathbf{e}}_2$, and $\hat{\mathbf{e}}_3$ are the unit vectors along the respective directions *x*, *y*, and *z*.

In the effective-mass approximation[14] (EMA) the wave function $|\psi\rangle$ is written as $|\Psi\rangle=\Sigma_{i=1}^{8}f_i|\mathbf{i}\rangle$, where the f_i's are slowly varying envelope functions of $|\psi\rangle$. Similarly within this single-particle approximation, the Hamiltonian of the system is given by $H'=H(\mathbf{K})+V(x)I$, where I is an 8×8 identity matrix, $\mathbf{K}=-i\nabla$, and $V(x)$ denotes the self-consistent potential felt by an electron in the space-charge layer near the interface. In the absence of a magnetic field, for an ideal interface where roughness is neglected and impurities are distributed uniformly, the total Hamiltonian is translationally invariant in the *yz* plane and the component $\mathbf{K}_\parallel$ in this plane is conserved. Hence, $\mathbf{K}_\parallel=k_y\hat{\mathbf{e}}_2+k_z\hat{\mathbf{e}}_3$ is a constant vector and may simply be written as $k_y\hat{\mathbf{e}}_2$ by choosing the direction of $\mathbf{K}_\parallel$ to coincide with $\hat{\mathbf{e}}_2$; henceforth we let $k_z=0$ in H' and simply denote $\mathbf{K}_\parallel$ by $\mathbf{k}$.

The Schrödinger equation

$$H'|\Psi\rangle=E|\Psi\rangle, \tag{1}$$

which is a set of eight coupled first-order differential equations for the envelope functions f_1, $f_2,\ldots f_8$ breaks into two subsets of equations, of lower dimension, given by

$$H^{(u)}|\Psi^{(u)}\rangle=E|\Psi^{(u)}\rangle, \tag{2a}$$

$$H^{(d)}|\Psi^{(d)}\rangle=E|\Psi^{(d)}\rangle. \tag{2b}$$

The Hamiltonian H' and wave function $|\psi\rangle$ are given by the direct sums $H^{(u)}\oplus H^{(d)}$ and $|\psi^{(u)}\rangle\oplus|\psi^{(d)}\rangle$, respectively. Note that $H^{(u)}$ and $H^{(d)}$ are related to one another by the relation $H^{(u)}(\mathbf{k})=H^{(d)}(-\mathbf{k})$, similarly for a given energy E the four-spinors $|\psi^{(u)}\rangle$ and $|\psi^{(d)}\rangle$ turn into each other, apart from a phase factor taken to be unity, if we make the transformation $\{u,\mathbf{k}\}\rightarrow\{d,-\mathbf{k}\}$. This important property, which is nothing more than Kramer's theorem applied to H', simplifies the writing of computer codes when solving the problem self-consistently. From now on we focus on Eq. (2a) for $|\psi^{(u)}\rangle$ since Eq. (2b) can be obtained from it by the aforementioned transformation.

In the local-density approximation[15] LDA $V(x)$ is written as:

$$V(X)=V_H(X)+V_{\rm im}(X)+V_{\rm xc}(X), \tag{3}$$

where $V_H(x)$, $V_{\rm im}(x)$, and $V_{\rm xc}(x)$ are the Hartree, image, and exchange-correlation potentials, respectively. Based on the results of prior works[7] we neglect the effects of $V_{\rm im}(x)$ and $V_{\rm xc}(x)$; these approximations help make the problem more manageable without losing the main physics. Moreover, the effect of impurities on the band-gap narrowing will be ignored at the doping levels considered.

The Hartree potential $V_H(x)$ satisfies the Poisson equation

$$\frac{d^2}{dx^2}V_H(x)=-\frac{4\pi e^2}{\epsilon_s}[\rho_{\rm inv}(x)+\rho_{\rm dep}], \tag{4}$$

where ϵ_s is the static dielectric constant of the semiconductor, $\rho_{\rm inv}(x)$ is the electron density due to the inversion electrons, and $\rho_{\rm dep}$ is the density of ionized impurities assumed to be uniform. The induced electron density $\rho_{\rm inv}(x)$ may be written as

$$\rho_{\rm inv}=\sum_{E\leqslant E_F}|\Psi^{(u)}|^2+|\Psi^{(d)}|^2=\rho_{\rm inv}^{(u)}(x)+\rho_{\rm inv}^{(d)}(x), \tag{5}$$

where the summation runs over all occupied surface bound states. We assume that $T=0$ K; therefore, only the lowest states are occupied; this assumption is justified by the experiment[4] to which the present theory is to be applied. The bound electrons of the inversion layer are described by two kinds of states[8] $|\psi_{\nu k}^{(u)}\rangle$ and $|\psi_{\nu k}^{(d)}\rangle$, where ν is the subband index, a new quantum number which ranges over the integer values {0,1,...} and k is the in-plane wave vector already defined and restricted to the first Brillouin zone. With this notation $\rho_{\rm inv}^{(u)}(x)$ and $\rho_{\rm inv}^{(d)}(x)$ become

$$\rho_{\rm inv}^{(u)}(x)=\frac{S}{2\pi}\sum_{\nu}\int_0^{K_F^{(\nu u)}}|\Psi_{\nu k}^{(u)}|^2k\,dk, \tag{6a}$$

$$\rho_{\rm inv}^{(d)}(x)=\frac{S}{2\pi}\sum_{\nu}\int_0^{K_F^{(\nu d)}}|\Psi_{\nu k}^{(d)}|^2k\,dk. \tag{6b}$$

In Eqs. (6a) and (6b) the sums are over all occupied subbands, and $k_F^{(\nu u)}$ and $k_F^{(\nu d)}$, are the Fermi wave vectors of the νth subband for species (u) and (d), respectively, while S is the lateral surface area. The Fermi wave vectors satisfy the relation $E_F=E_{\nu i}(k_F^{(\nu i)})$, where E_F is the Fermi energy of the 2D electron gas and $E_{\nu i}(k)$, with $i=u$ or d, is the energy spectrum of subband ν and species (i).

We write $|\psi^{(u)}\rangle$ as ${}^t(\varphi_1^{(u)},\ \varphi_2^{(u)},\ \varphi_3^{(u)},\ \varphi_4^{(u)})$ with $\varphi_1^{(u)},\ldots,\varphi_4^{(u)}$ being slowly varying envelope functions standing for the components of the 4-spinor $|\psi^{(u)}\rangle$ on the relevant basis (see Appendix A) and ${}^t(\cdots)$ standing for the transpose operation, for $|\psi^{(d)}\rangle$ replace (u) by (d) everywhere. In Eqs.

(6a) and (6b) for $\rho_{\rm inv}^{(u)}(x)$ and $\rho_{\rm inv}^{(d)}(x)$, the probability densities $|\psi_{\nu k}^{(u)}|^2$ and $|\psi_{\nu k}^{(d)}|^2$ then become

$$|\Psi_{\nu k}^{(u)}(x)|^2=\sum_{i=1}^{4}|\varphi_{i,\nu k}^{(u)}(x)|^2, \tag{7a}$$

$$|\Psi_{\nu k}^{(d)}(x)|^2=\sum_{i=1}^{4}|\varphi_{i,\nu k}^{(d)}(x)|^2. \tag{7b}$$

Note that the density is k dependent since the components $\varphi_1,\varphi_2,\ldots$ of the 4-spinors $|\Psi^{k(u)}\rangle$ and $|\Psi^{k(d)}\rangle$ are k dependent.

Far away from the interface the effects of the gate voltage are screened by the charge distribution and the electric field vanishes beyond the depletion layer depth d defined through $V_H'(d)=0$. Using this condition and $V_H(0)=0$ as BC for $V_H(x)$, the Hartree potential may then be written in its integral representation as

$$V_H(x)=\frac{4\pi e^2}{\epsilon_s}\left\{(N_{\rm inv}+N_{\rm dep})x-\frac{N_{\rm dep}}{2d}x^2-\int_0^x(x-x')\rho_{\rm inv}(x')dx'\right\}. \tag{8}$$

In Eq. (8) for $V_H(x)$, $N_{\rm inv}=\int_0^d\rho_{\rm inv}(x)dx$ and $N_{\rm dep}=d(N_A-N_D)$ are the areal electronic density in the inversion layer and the surface density of ionized impurities, respectively, with N_A and N_D being the volume densities of acceptors and donors, respectively. The depletion layer depth d defined previously is given by

$$d^2=\frac{2}{|N_D-N_A|}\left(\frac{\epsilon_s}{4\pi e^2}(E_F+\varepsilon_g/2)-\int_0^\infty x\rho_{\rm inv}(x)dx\right), \tag{9}$$

Equations (3)–(9), together with the Schrödinger equation (1), form the basis of the zero-field treatment of the electronic structure in a NGS inversion layer. The equations are somewhat complicated and their solution necessitates elaborate self-consistent computations that are performed numerically. To solve the self-consistent problem we proceed in the following way. We first write $\varphi_1^{(u)}$ in the following form:

$$\varphi_1^{(u)}=g(x)A_u(x)\frac{e^{iky}}{\sqrt{S}} \tag{10}$$

with $g(x)$ being given by

$$g(x)=\left|\frac{[\varepsilon_g/2+E-V(x)][\varepsilon_g/2+\Delta+E-V(x)]}{[\varepsilon_g/2+2\Delta/3+E-V(x)]}\right|^{1/2} \tag{11}$$

and $A_u(x)$ an unknown function satisfying the equation

$$\frac{d^2}{dx^2}A_u(x)+Q_u(x)A_u(x)=0. \tag{12}$$

In Eq. (11) for $g(x)$, ε_g and Δ are, respectively, the energy gap between the Γ_6 and Γ_8 bands on the one hand and the spin-orbit splitting between the Γ_7 and Γ_8 bands on the other, with Γ_6, Γ_8, and Γ_7 being, respectively, the lowest conduction bands, the topmost valence bands, and the split-off bands.

In Eq. (12), note that the ''reduced wave amplitude'' $A_u(x)$ depends both on E and k; moreover, the same equation may be thought of as a one-dimensional (1D) Schrödinger equation with $Q_u(x)$ being a squared wave vector which is x, E, and k dependent and given by

$$Q_u(x)=\beta_u(x)+\alpha_1(x)\frac{d}{dx}\ln|g(x)|+\frac{1}{g(x)}\frac{d^2}{dx^2}g(x) \tag{13}$$

with the new functions $\alpha_1(x)$ and $\beta_u(x)$ given by

$$\alpha_1(x)=\frac{dV(x)}{dx}\left(\frac{1}{\varepsilon_g/2+E-V(x)}+\frac{1}{\varepsilon_g/2+\Delta+E-V(x)}-\frac{1}{\varepsilon_g/2+E+2\Delta/3-V(x)}\right), \tag{14}$$

$$\beta_u(x)=\frac{[E-V(x)]^2-\varepsilon_g^2/4}{\frac{2}{3}P^2}\Xi(\Delta)+\frac{\frac{1}{2}kV'(x)}{\varepsilon_g/2+E-V(x)}\Theta(\Delta)-k^2, \tag{15}$$

where $\Xi(\Delta)$ and $\Theta(\Delta)$ are

$$\Xi(\Delta)=\frac{\Delta+E+\varepsilon_g/2-V(x)}{\Delta+3/2[E-V(x)+\varepsilon_g/2]},$$

$$\Theta(\Delta)=\frac{\frac{4}{3}\Delta[\varepsilon_g/2+E-V(x)+\Delta/2]}{[\varepsilon_g/2+\Delta+E-V(x)][\varepsilon_g/2+E-V(x)+2\Delta/3]}.$$

In Eq. (15) for $\beta_u(x)$ the new parameter $P=-i\hbar/m\langle S|P_z|z\rangle$ is simply Kane's momentum matrix element with m being the free-electron mass. In the six-band model $\Delta\to\infty$, $\Xi(\Delta)$ and $\Theta(\Delta)$ tend to 1 and these expressions take a much simpler form,

$$g(x)\to|3[\varepsilon_g/2+E-V(x)]/2|^{1/2}, \tag{11'}$$

$$\alpha_1(x)\to\frac{V'(x)}{\varepsilon_g/2+E-V(x)}, \tag{14'}$$

$$\beta_u(x)\to\frac{[E-V(x)]^2-\varepsilon_g^2/4}{\frac{2}{3}P^2}-k^2+\frac{1}{2}\frac{kV'(x)}{\varepsilon_g/2+E-V(x)}. \tag{15'}$$

In the four-band model the equations are

$$g(x)\to\sqrt{\varepsilon_g/2+E-V(x)}, \tag{11''}$$

$$\beta(x)\to\frac{[E-V(x)]^2-\varepsilon_g^2/4}{P^2}-k^2, \tag{15''}$$

$$\alpha_1(x)\to\frac{V'(x)}{\varepsilon_g/2+E-V(x)}. \tag{14''}$$

B. Self-consistent computations

Consider Eq. (12) for the ''reduced wave amplitude'' $A_u(x)$, which is essentially a 1D second-order differential equation with two parameters E and k, and look for solutions satisfying the proper BC at the interface (Appendix A) and vanishing at $x=+\infty$. The *ad hoc* BC at $x=+\infty$ is imposed on physical grounds only because the electrons in the inversion layer are bound to the surface and are not likely to ''stray away'' very far from it. In other words, this approximation neglects tunneling[16] from the conduction band into the valence bands, although tunneling into the gap is partially allowed, and is expected to break down when the forbidden gap ε_g becomes very small as the case is in the NGS compound $Hg_{1-x}Cd_xTe$ as the Cd content diminishes and x approaches zero. No effort will be spent on considering the effects of tunneling on the electronic structure.

Let x_1 be the classical turning point defined by $Q_u(x_1)=0$. Then in the classically allowed region defined by $0<x\leqslant x_1$, where $Q_u(x)>0$, the semiclassical solution of Eq. (12) is[17]

$$A_u(x)\propto\sqrt{\frac{8\pi\zeta}{3Q_u^{1/2}}}\left\{\cos\left(\eta+\frac{\pi}{3}\right)J_{1/3}(\zeta)+\cos\left(\frac{\pi}{3}-\eta\right)J_{-1/3}(\zeta)\right\},\tag{16}$$

where the ''phase'' $\zeta(x)$ is given by $\zeta=\int_x^{x_1}\sqrt{Q_u(x')}dx'$, and η is a real constant. In the classically forbidden region, defined by $x\geqslant x_1$ and where $Q_u(x)<0$, the solution is given by[17]

$$A_u(x)\propto\sqrt{\frac{8|\zeta|}{\pi|Q_u|^{1/2}}}\left[\pi\sin(\eta)I_{1/3}(|\zeta|)+2\cos\left(\frac{\pi}{3}-\eta\right)K_{1/3}(|\zeta|)\right],\tag{16'}$$

with $\zeta(x)$ given by $\zeta=\int_{x_1}^{x}\sqrt{|Q_u(x')|}dx'$. In both cases the ''phase'' $\zeta(x)$ is E and k dependent since both $Q_u(x)$ and x_1 are. In Eq. (16) for $A_u(x)$, $J_{\pm1/3}$ are Bessel functions of the first kind of order $\pm1/3$, similarly in Eq. (16') $K_{1/3}$ and $I_{1/3}$ are modified Bessel functions of the same order.[18] These functions are distinct from the Airy functions Ai and Bi although they are related to them through well-known expressions.[18] For an argument u real and large the modified Bessel functions $K_\nu(u)$ and $I_\nu(u)$ have the asymptotic behaviors[18] $I_\nu(u)\sim e^u\Upsilon_1(u)$ and $K_\nu(u)\sim e^{-u}\Upsilon_2(u)$, where $\Upsilon_1(u)$ and $\Upsilon_2(u)$ are regular functions of u. Since $\zeta(x)$ is a positive and increasing function of x, we define the bound states of H' by setting η to zero to eliminate the diverging term in Eq. (16'). In the classically forbidden region $A_u(x)$ takes on the form

$$A_u(x)\propto 2\left(\frac{8|\zeta|}{\pi|Q_u|^{1/2}}\right)^{1/2}K_{1/3}(|\zeta|)\tag{17}$$

with a corresponding form in the classically allowed region

$$A_u(x)\propto\sqrt{\frac{8\pi\zeta}{3Q_u^{1/2}}}\{J_{1/3}(\zeta)+J_{-1/3}(\zeta)\}.\tag{17'}$$

At the interface the total wave function $|\Psi^{(u)}>$ vanishes identically in the whole plane $x=0$; this requirement imposes on $A_u(x)$ the following BC:

$$\left.\frac{1}{A_u}\frac{dA_u}{dx}\right|_{x=0}=G(E,k),\tag{18}$$

where $G(E,k)$ is an E and k-dependent function given by

$$G(E,k)=\frac{e\mathcal{E}_x(0)}{2}\Gamma_1(\Delta)-\frac{k}{2}\Gamma_2(\Delta)+\frac{1}{\sqrt{2/3}P}(E+\varepsilon_g/2)\Xi(\Delta)\tag{19a}$$

and the new functions $\Gamma_1(\Delta)$ and $\Gamma_2(\Delta)$ are written as

$$\Gamma_1(\Delta)=\frac{\frac{2}{3}\Delta^2+\frac{4}{3}\Delta(E+\varepsilon_g/2)+(E+\varepsilon_g/2)^2}{(E+\varepsilon_g/2+\frac{2}{3}\Delta)(E+\varepsilon_g/2+\Delta)(E+\varepsilon_g/2)},\tag{19b}$$

$$\Gamma_2(\Delta)=\frac{\Delta}{\Delta+\frac{3}{2}(E+\varepsilon_g/2)},\tag{19c}$$

with the already defined function $\Xi(\Delta)$ to be evaluated at $x=0$.

In the six-band model the expressions for $\Gamma_1(\Delta)$ and $\Gamma_2(\Delta)$ are obtained by taking the limit $\Delta\to\infty$ while in the four-band model one must set Δ to 0 in the expressions for $\Gamma_1(\Delta)$ and $\Gamma_2(\Delta)$ and replace P by $P'=3/2P$. In Eq. (19a) for $G(E,k)$, e is the proton charge and $\mathcal{E}_x(0)$ is the electric-field strength right at the interface. Although the right-hand side of Eq. (18) involves the electric field at the interface only, the spectrum depends on the self-consistent potential in the whole inversion layer because both x_1 and ζ depend on it there, too.

For a given potential $V(x)$, the use of the semiclassical expression for $A_u(x)$, given by Eq. (17'), in Eq. (18) combined with Eqs. (19a)–(19c) results in a highly nonlinear eigenvalue equation for E where the wave vector k enters as a parameter. The values of $E(k)$ obtained in this way are approximate, but within a meV or so of the exact value; nonetheless, they need to be refined later in order to get the right wave functions which are very energy sensitive; this approximate subband structure is nevertheless very useful in obtaining the right subband structure for an otherwise very complex numerical problem. The parameters ϵ_s, ε_g, Δ, and P are fixed by the choice of the material and taken to be those of bulk. The extensive amount of experimental data on InSb (Ref. 4) led us to choose it for our numerical computations. Moreover, for simplicity we use the six-band model by dropping the split-off band (i.e., we let $\Delta\to\infty$), in this approximation the bulk effective mass at the Γ point is given by $\hbar^2/2m^*=2P^2/3\varepsilon_g$.

The self-consistent calculations proceed in the following way. For a given areal electronic density $N_{\rm inv}$ we make a first guess, e.g., triangular potential;[5] for $V(x)$ to start the computations; this allows us to find the energy spectrum, the wave functions $|\Psi_{\nu k}^{(u)}\rangle$ and $|\Psi_{\nu k}^{(d)}\rangle$, the Fermi energy E_f, and the depletion layer depth d. The electronic density is then

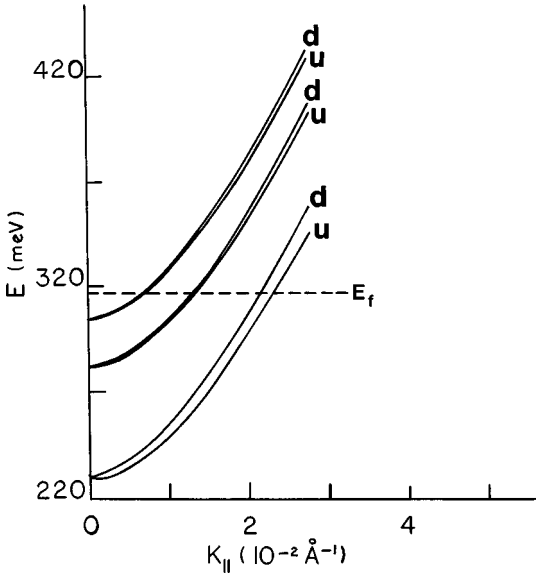

FIG. 1. Subband structure of electrons in the inversion layer, in the absence of a magnetic field, with the Fermi energy E_F and the wave vector along the interface $K_{\|}$; the indices (u) and (d) are explained in the text.

evaluated and used in Eq. (8) to compute the new potential $V(x)$ which will then be used in the next iteration until self-consistency is reached. To make the numerical calculations stable it is useful to use the scheme $V_{\rm in}^{(n+1)}=V_{\rm in}^{(n)}+\lambda(V_{\rm out}^{(n)}-V_{\rm in}^{(n)})$,[5] where $0<\lambda<1$, and $V_{\rm in}^{(m)}$ and $V_{\rm out}^{(m)}$ are the input and output potentials in the mth iteration, respectively. In practice, we start with $\lambda\approx 0.3$ and then increase λ toward 1 as self-consistency approaches. For a given potential $V(x)$, i.e., within a given iteration, we first look for the spectrum within the semiclassical approximation and then later refine the results using a bracketing algorithm; the parameters[19] used are $\varepsilon_g=236.8$ meV for the direct gap, $m^*=0.0139\,m$ for the bulk band-edge mass, $\epsilon_s=17.8$ for the static dielectric constant, and $|N_A-N_D|=3\times10^{14}\,\mathrm{cm}^{-3}$ (Ref. 4) for the density of the ionized uncompensated impurities.

C. Results and discussion

This section presents the results of our self-consistent computations and checks them against available experimental data found in the published literature. The comparison serves as a test of the complex self-consistent calculations and allows us to make some assessments about the self-consistent potential to which the electrons in the inversion layer are submitted.

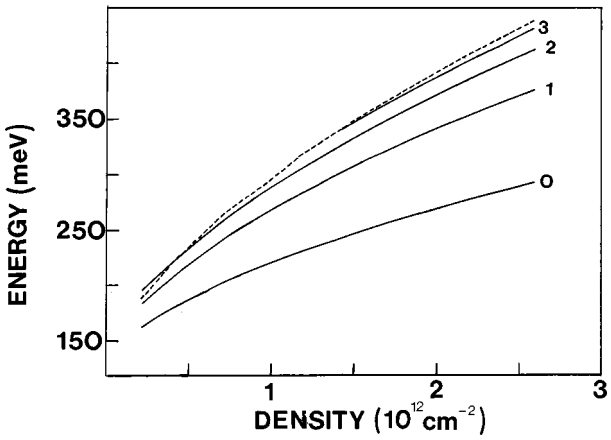

FIG. 2. Subband energy at $K_{\|}=0$ as a function of areal electron density $N_{\rm inv}$. The indices 0, 1, .., denote the subband and the dashed curve represents the Fermi energy.

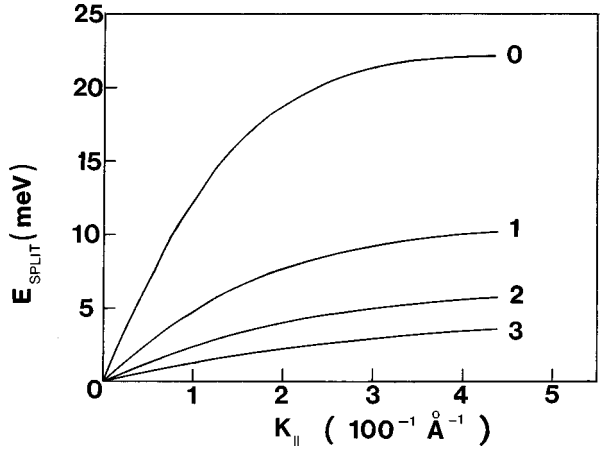

FIG. 3. Electric-field-induced splitting $[E_\nu^{(d)}(k)-E_\nu^{(u)}(k)]$, as a function of the in-plane wave vector; the indices 0, 1, .., denote the subbands.

Figure 1 shows a typical subband structure calculated with the present theory; very clearly seen is the spin splitting of the subbands caused by the strong surface electric field. In Fig. 2 we plot $E_\nu^{u,d}(k=0)$ as a function of the areal electron density $N_{\rm inv}$ for the subband index ν ranging from 0 to 3. Also shown in dashes is the Fermi energy E_F whose intersection with the solid lines labeled by ν indicates at which density a given subband starts to be populated. For a given density $N_{\rm inv}$ we define the spin splitting within a given subband ν as $\Delta E(k)=E_\nu^{(d)}(k)-E_\nu^{(u)}(k)$. In Fig. 3 we show this spin splitting ΔE as a function of the in-plane wave vector k for $N_{\rm inv}=2.59\times10^{12}\,\mathrm{cm}^{-2}$. Note how the spin splitting diminishes as the subband index increases; note also how it increases with k and reaches rather large values in the order of a few tens of meV. In Fig. 4 we display our calculated subband occupancies n_ν as a function of $N_{\rm inv}$. The subband

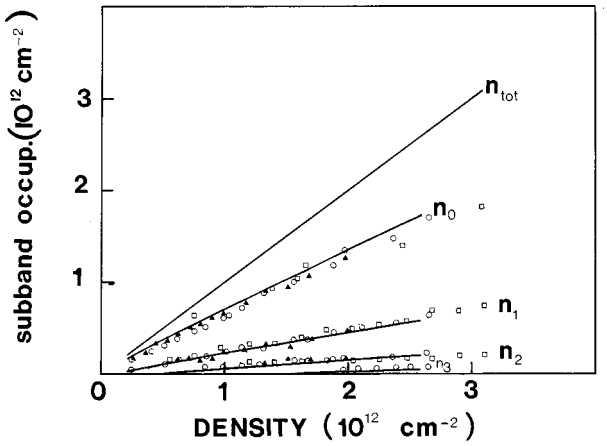

FIG. 4. Theoretical subband occupancies (solid lines) along with the experimental subband occupancies taken from Ref. 4. $n_0, n_1, \ldots, n_3$ are, respectively, the occupancies of the zeroth, first,... and third subbands.

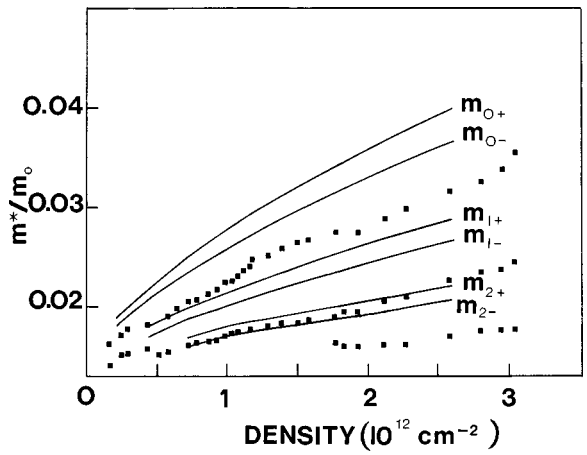

FIG. 5. Calculated spin split density-of-state (DOS) mass m^*_{va} (solid lines) along with the measured CR masses (■) taken from Ref. 4 as a function of the areal electron density $N_{\rm inv}$.

occupancy n_ν is computed using $n_\nu=(1/2\pi)(k_f^{(\nu u)^2}+k_f^{(\nu d)^2})$, where $k_f^{(\nu u)}$ and $k_f^{(\nu d)}$ are defined in Sec. II A. Also shown on the same figure are experimental data points taken from Ref. 4 for three different sets of samples. It is clear that agreement is excellent over the whole range of $N_{\rm inv}$, i.e., from $0.21\times10^{12}\,{\rm cm}^{-2}$ to about $2.59\times10^{12}\,{\rm cm}^{-2}$; however, the experimental data seem to show some structure, as $N_{\rm inv}$ is varied, which the present computation does not reproduce. We believe that this structure originates entirely from the presence of the finite magnetic field present in the SdH experiments used to deduce the subband occupancies. We define a subband density-of-state mass $m^*_{\nu\sigma}$ with σ being equal to (u) or (d), evaluated at the Fermi level, as

$$m^*_{\nu\sigma}=\hbar^2 k_F^{(\nu\sigma)}\left(\frac{\partial E_{\nu\sigma}(k)}{\partial k}\right)^{-1}_{k=k_F^{(\nu\sigma)}}.$$

It is clear that $m^*_{\nu\sigma}$ depends on the subband index, the spin index, and the electron density $N_{\rm inv}$. In Fig. 5 we display the calculated subband density of state mass together with the experimental CR mass as measured in Ref. 4. Three important features should be commented on here. (1) All calculated masses occur in doublets, thus reflecting a noticeable difference in mass for each branch (u or d) of the spin split subband. (2) The subband mass $m^*_{\nu\sigma}$ is very subband dependent, which is a well-known characteristic of NGS and can be traced back to the nonparabolicity of the 3D band structure. (3) All masses $m^*_{\nu\sigma}$ are monotonously increasing functions of $N_{\rm inv}$. On the other hand, the experimental masses, as deduced in the same reference, show the following prominent aspects: (1) there is a set of three different masses, each of which corresponds to a given subband, (2) the masses increase steadily as $N_{\rm inv}$ increases, and (3) the mass, especially in the zeroth subband, shows a marked oscillatory behavior superimposed on its steady increase. We now comment on these important issues. First, the discrepancy between the calculated density-of-state (DOS) mass and the experimental CR mass is rather large; second, the DOS mass shows no oscillatory behavior; and third the latter is spin split whereas the experimental CR mass is not. These results show that unlike the situation in a wide gap semiconductor, in a NGS it is just inadequate to compare the zero-field mass $m^*_{\nu\sigma}$ with finite field CR mass, a practice which has been widely adopted. This result demonstrates clearly the necessity of including the effects of the magnetic field in the whole picture.

III. FINITE FIELD TREATMENT

A. Formulation of the problem

Consider now the problem of the electronic structure in the presence of a finite magnetic field. For later convenience we consider two frames of reference $\{x,y,z\}$ and $\{X,Y,Z\}$ denoted by (a) and (b), respectively. Frames (a) and (b) are related to one another by the identities $x\equiv Z$, $y\equiv X$, $z\equiv Y$. Frame (a) is convenient for the study of electrons in the absence of a normal magnetic field and is the one used in Sec. II. On the other hand, because the natural direction for quantizing angular momentum is the one provided by the magnetic field **B**, frame (b) is the frame of choice for studying the electronic structure in the presence of a **B** field. As the need arises we will make use of either frame.

As in the preceding sections the semiconductor occupies the right-hand side and the insulator the left-hand side with the magnetic field **B** being normal to the interface and pointing in the positive Z direction. The eight-band Kane model, with all the quadratic k terms being neglected, is used within the EMA; moreover, the self-consistent potential $V(Z)$ is assumed to be independent of the magnetic field B. In the EMA H', the one-particle Hamiltonian of the system, may be written as $H(\mathbf{k})+IV(Z)$, where I is the identity operator and $H(\mathbf{k})$ is the Kane Hamiltonian with the correspondence $\mathbf{k}\rightarrow-i\nabla+e/\hbar c\mathbf{A}$ being made. Note that in H' both $H(\mathbf{k})$ and I are 8×8 matrix operators written on the basis vectors $\{|\mathbf{1}\rangle,...,|\mathbf{8}\rangle\}$ of Appendix A where lowercase letters are, however, replaced by uppercase ones because of cubic symmetry. We introduce the vector potential **A** which we write in the Landau gauge as $(-BY,0,0)$; furthermore, we define the creation and annihilation operators a and $a^\dagger$ by $-s(k_X+ik_Y)/\sqrt{2}$ and $-s(k_X-ik_Y)/\sqrt{2}$, respectively, with the cyclotron radius s being given by $(c\hbar/eB)^{1/2}$. The operators a and $a^\dagger$ in terms of which we express the operator **k** given above satisfy the commutation relation $[a,a^\dagger]=1$. In addition, $a^\dagger\chi_n=\sqrt{n+1}\chi_{n+1}$ and $a\chi_n=\sqrt{n}\chi_{n-1}$, where $\chi_n(Y-Y_0)$ is the harmonic-oscillator wave function of order n centered at $Y_0=s^2k_X$; in the expression giving Y_0, k_X is the wave vector along the X direction which is conserved because of our choice of gauge.

To alleviate the notation we will drop the subscript X from k_X and denote it simply by k; the new quantum numbers, in the presence a magnetic field, then become ν, n, k and σ with n being the Landau index of the state and σ the spin which we quantize along Z. As before ν denotes the subband, note that n ranges over the set of integer values $\{-1,0,1,2,...\}$, and the convention of Ref. 8 is used, i.e., the Landau index of a given state refers to the Landau index of the first component of its spinor and the component of the spinor is taken to be identically zero if the oscillator wave function $\chi_{n'}(Y-Y_0)$ for that component involves a negative

index n'. As for σ it can take on one of two values ± 1, denoted $\pm$, and k is limited to the first Brillouin zone.

The eigenstate $\Phi_{\nu nk\sigma}$ of H' satisfies the Schrödinger equation

$$H'\Phi_{\nu nk\sigma}=E\Phi_{\nu nk\sigma}. \tag{20}$$

With L denoting the length of the sample in the X direction, $\Phi_{\nu nk\sigma}$ is written as

$$\Phi_{\nu nk\sigma}=\frac{e^{ikX}}{\sqrt{L}}{}^{t}(F_1\chi_{n'},F_2\chi_{n+1'},F_3\chi_{n-1'},F_4\chi_{n'},F_5\chi_{n+1'},F_6\chi_{n+2'},F_7\chi_{n'},F_8\chi_{n+1}), \tag{21}$$

where $\{F_j\}$ for $j=1,...,8$ are Z-dependent slowly varying envelopes functions, which depend on the three indices ν, n, and σ; because of the presence of the electric field in the space-charge layer and also because of the special BC at $Z=0$, solving Eq. (20) is not a trivial task. As it stands Eq. (20) is a set of eight first-order differential equations which we solve as follows: First Eq. (21) for $\Phi_{\nu nk\sigma}$ is plugged into Schrödinger's equation, Eq. (20), which turns into

$$h^{(n)}\xi_{\nu n\sigma}=E\xi_{\nu n\sigma}, \tag{22}$$

where $h^{(n)}$ is an 8×8 matrix operator and $\xi_{\nu n\sigma}(Z)$ is given by

$$\xi_{\nu n\sigma}(Z)={}^{t}(F_1,F_2,F_3,F_4,F_5,F_6,F_7,F_8). \tag{23}$$

Now let $\tilde{h}^{(n)}=Uh^{(n)}U^{\dagger}$ and $\overline{\xi}=U\xi$ be the transforms of $h^{(n)}$ and ξ, respectively, by the unitary transformation U given by

$$U=\begin{pmatrix}\Pi_1 & 0 & 0\\ 0 & \Pi_2 & 0\\ 0 & 0 & \Pi_1\end{pmatrix}. \tag{24}$$

In Eq. (24) for U, 0 stands for a nil matrix of appropriate dimensions (i.e., 2×2, 2×4, or 4×2) and Π_1 and Π_2 are given by

$$\Pi_1=\frac{1}{2}\begin{pmatrix}-\alpha & -\alpha\\ \alpha^* & -\alpha^*\end{pmatrix},$$

$$\Pi_2=\frac{1}{4}\begin{pmatrix}\alpha^* & \sqrt{3}\alpha^* & \sqrt{3}\alpha^* & \alpha^*\\ \sqrt{3}\alpha & \alpha & -\alpha & -\sqrt{3}\alpha\\ -\sqrt{3}\alpha^* & \alpha^* & \alpha^* & -\sqrt{3}\alpha^*\\ -\alpha & \sqrt{3}\alpha & -\sqrt{3}\alpha & \alpha\end{pmatrix} \tag{25}$$

with $\alpha=1+i$. We write $\tilde{h}^{(n)}$ explicitly as

$$\tilde{h}^{(n)}=\begin{pmatrix}\mathcal{H}_0^{(+)} & 0\\ 0 & \mathcal{H}_0^{(-)}\end{pmatrix}+\gamma\begin{pmatrix}R & 0\\ 0 & -R\end{pmatrix}+\delta\begin{pmatrix}0 & R\\ R & 0\end{pmatrix} \tag{26}$$

with

$$R=\begin{pmatrix}0 & i & i\sqrt{3} & 0\\ -i & 0 & 0 & 0\\ -i\sqrt{3} & 0 & 0 & 0\\ 0 & 0 & 0 & 0\end{pmatrix},$$

$$\text{where}\quad \gamma=\frac{P}{4s}(2\sqrt{n+1}-\sqrt{n}-\sqrt{n+2})$$

$$\text{and}\quad \delta=\frac{P}{4s}(\sqrt{n+2}-\sqrt{n}). \tag{27}$$

In Eq. (26) $\mathcal{H}_0=\mathcal{H}_0^{(+)}\oplus\mathcal{H}_0^{(-)}$, the first part of $\tilde{h}^{(n)}$ describes the semiclassical effects while the second and third terms describe the quantum contributions. Note that the Hermitian 4×4 matrix R, with eigenvalues $\{0,\pm 2\}$, is constant. The importance of the quantum corrections are all included within the coupling constants δ and γ, which both tend to 0 as the magnetic field B vanishes or as n increases towards infinity. In practice the lowest levels (with small n) are the only ones of interest and one has to consider the quantum contributions very seriously because their effect is far from being small. Moreover, although both coupling constants tend to vanish for large n, the contribution of the last term is always dominant.

Let $|\zeta_{\nu n\sigma}\rangle$ be an eigenstate of $\mathcal{H}_0$ with eigenvalue $\epsilon_{\nu n\sigma}$. Then, because $\mathcal{H}_0$ is already block diagonal, its eigenstates $|\zeta_{\nu n\sigma}\rangle$ can be obtained from the 4-spinors of Sec. II by making the substitution $k\rightarrow-\sqrt{2(n+1)}/s$. For n fixed the states $|\zeta_{\nu n\sigma}\rangle$ satisfy the orthogonality relation $\langle\zeta_{\nu n\sigma}|\zeta_{\nu' n\sigma'}\rangle=\delta_{\nu\nu'}\delta_{\sigma\sigma'}$, and form, therefore, a convenient basis in terms of which the eigenstates $|\overline{\xi}_{\nu n\sigma}\rangle$ of $\tilde{h}^{(n)}$ can be expanded as

$$|\overline{\xi}_{\nu n\sigma}\rangle=\sum_{\nu'\sigma'}C_{\nu'\sigma',\nu\sigma}|\zeta_{\nu' n\sigma'}\rangle, \tag{28}$$

where the complex expansion coefficients are to be determined. Hence, the eigenvalue problem becomes

$$(\epsilon_{\nu n\sigma}-E)C_{\nu\sigma,\nu\sigma}+\sum_{\nu'=0;\sigma'=\pm 1}^{\infty}\langle\zeta_{\nu n\sigma}|\mathcal{R}^{(n)}|\zeta_{\nu' n\sigma'}\rangle \times C_{\nu'\sigma',\nu\sigma}=0, \tag{29}$$

where we introduced the operator $\mathcal{R}^{(n)}=\tilde{h}^{(n)}-\mathcal{H}_0$.

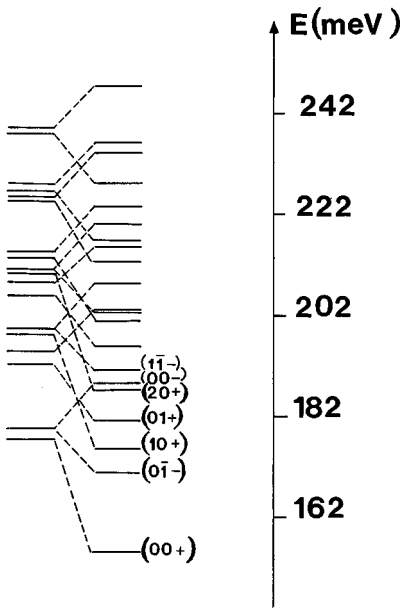

FIG. 6. Landau ladder in the presence of a finite normal magnetic field; the indices $(\nu n\,\sigma)$ are explained in the text and the doublet on the left represents the energy levels within the semiclassical approximation as defined in Sec. III.

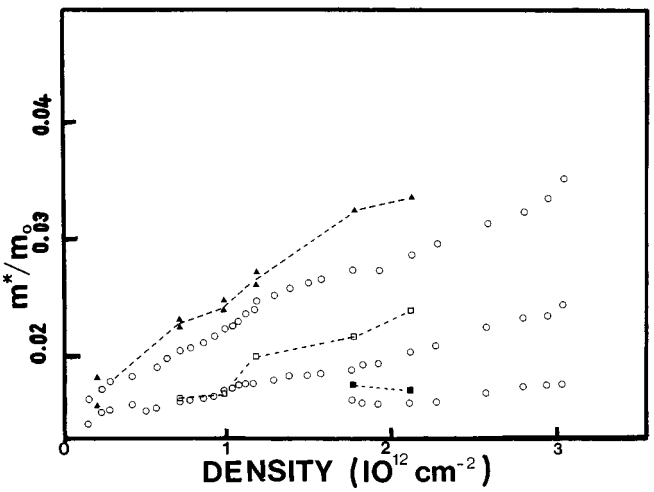

FIG. 7. Theoretical subband cyclotron resonance masses (▲, □, ■) along with the measured cyclotron resonance masses (○) of Ref. 4 for comparison. The abscissa represents the areal electron density in the inversion layer and the dashes are guides for the eye only.

B. Results and discussion

We solved Eq. (29) numerically proceeding in the following way: For a given density $N_{\rm inv}$, the self-consistent potential being that of Sec. II, we fix n and B. First we find the eigenvalues $\epsilon_{\nu n'\sigma}$ and eigenvectors $|\zeta_{\nu n'\sigma}\rangle$ of $\mathcal{H}_0$ for $\sigma=\pm$ (corresponding to u and d, respectively) and $\nu=0,...,5$, then we construct the matrix $\langle\zeta_{\nu' n\sigma'}|\mathcal{R}^{(n)}+\epsilon_{\nu n\sigma}I|\zeta_{\nu n\sigma}\rangle$ which we diagonalize numerically. The character of the resulting states is determined from the values of the dominant expansion coefficients. Note that convergence in the expansion given by Eq. (28) is assured because as ν increases the eigenfunctions $\zeta_{\nu n\sigma}(Z)$ oscillate more and more rapidly and this makes the influence of higher subbands on the lower ones (the ones actually populated) less and less effective because the overlap integrals defining the matrix elements of $\mathcal{R}^{(n)}$ become very small. By repeating this procedure for another value of n at the same magnetic-field strength B we get the whole spectrum. Since our aim is the interpretation of CR spectra, we restrict our computations only to those values of B extracted from CR traces at which resonance seems to occur. Our calculations of the Landau ladder cover the range $N_{\rm inv}=0.21\times10^{12}\,{\rm cm}^{-2}$ to $2.11\times10^{12}\,{\rm cm}^{-2}$ and at each density the computations are performed for a few B values. Figure 6 shows a typical Landau ladder, the doublet structure on the left exhibits the Landau levels (LL) in the semiclassical approximation (i.e., give $\epsilon_{\nu n\sigma}$) while those on the right include the quantum corrections already mentioned. The calculation is for $N_{\rm inv}=0.21\times10^{12}\,{\rm cm}^{-2}$ and $B\approx2.34\,{\rm T}$; the indices $(\nu n\sigma)$ identify the different LL with $\bar{1}$ denoting the case $n=-1$. It is worth noting the intricate structure of this energy spectrum which comes as a consequence of the very small bulk mass m^* and large g^* for InSb. Note, in particular, how LL from higher subbands, e.g., $(10+)$, are lower in energy than levels from lower subbands, e.g., $(01+)$ or $(00-)$. It is noteworthy to stress that the order in which the levels occur is important because it determines which LL the CR process will involve, and hence the corresponding effective mass. Based on our knowledge of the LL we identified the levels involved in the absorption process of the CR experiments reported in Ref. 4 (for details see Ref. 9). In the experiment[4] the authors use an infrared laser of energy $\hbar\omega=17.6\,{\rm meV}$ and sweep B to achieve resonance. In our identification of the lines we used the following guidelines: First we locate the position of the Fermi level and look for states above the Fermi level that can be coupled to states below it, then compute the energy difference between them and compare it to the laser energy. If the difference is not too great compared to the line broadening $\hbar/\tau$, the transition is considered resonant; otherwise, we look for states which are as close as possible to resonance. Use is made of the line broadenings: 3.25, 1.625, and 1.3 meV for the ground, first, and second subbands, respectively, as were reported and used to get the best fit in Ref. 4.

For $n\geqslant0$ the cyclotron mass is given by $m^*_{\nu n\sigma}=\hbar\omega/(E_{\nu n'\sigma}-E_{\nu n'-1\sigma})$, with $n'=n+\frac{1}{2}(1+\sigma)$ and $\sigma=\pm1$; $\omega=eB/mc$ being the angular cyclotron frequency of free electrons.

In Fig. 7 the calculated cyclotron mass $m^*_{\nu n\sigma}$ is shown together with the experimental results for comparison. First we notice that the $B=0$ masses $(m^*_{\nu\sigma})$ are larger than the $B\neq0$ masses for all values of $N_{\rm inv}$ contrary to what was believed,[14] as it was thought that the ''energy associated'' with B would add on to that due to the surface electric field alone and through nonparobolicity would lead to an increase of the effective mass. That conjecture is, of course, erroneous since it manifestly overlooks the variation of the Fermi energy with the magnetic field. The results exhibited in Fig. 7 deserve some discussion; in the second subband $(\nu=2)$ the calculated mass is m^*_{20-} in the two cases shown; note how the calculated mass shows a slight decrease as $N_{\rm inv}$ increases and thus follows remarkably well the trend of the experimental mass in contrast to the $B=0$ theory of Sec. II which predicts a spin-split mass and a steady increase of the latter.

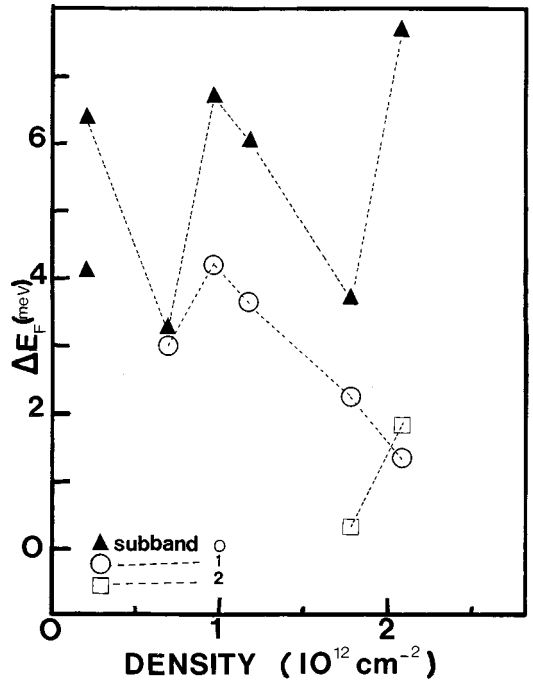

FIG. 8. Variations of $\Delta E_F = E_F(B=0) - E_F(B\neq 0)$ as a function of the areal electron density $N_{\rm inv}$; dashes are guides for the eyes.

In the first subband ($\nu=1$) the calculated masses at $N_{\rm inv} = 0.71\times 10^{12}\,{\rm cm}^{-2}$ and $0.98\times 10^{12}\,{\rm cm}^{-2}$ coincide with the experimental masses. At higher densities we note, however, less agreement with experiment. Nonetheless, the trend as well as the superimposed structure of the experimental mass are reproduced and the calculated mass is brought closer to the experimental one. We note in passing that at $N_{\rm inv}=1.17\times 10^{12}\,{\rm cm}^{-2}$ the calculated masses represent m^*_{11+} and m^*_{10-} which are equal, within our numerical accuracy; at higher densities, on the other hand, the calculated masses represent a single LL. In the ground subband ($\nu=0$) the calculated masses show a steady increase with some structure that follows quite well the experimental one; a doublet structure is also present at densities below $1.77\times 10^{12}\,{\rm cm}^{-2}$. The fit of Ref. 4 uses only one mass per subband as a fitting parameter and thus cannot predict multiple masses for each subband. It is also of interest to note the stronger structure in the ground subband which mainly comes as a result of the stronger magnetic fields required to achieve CR. These strong magnetic fields produce large oscillations of the Fermi energy around its value in the absence of the magnetic field as is very clearly seen in Fig. 8. These oscillations in E_F are reproduced in the CR mass through two mechanisms. First, the oscillations of E_F determine which of the LL are capable of contributing to the absorption process through the interplay of the filling factor of the levels, the selection rules, the Pauli exclusion principle, and the resonance condition. Second, the nonparabolicity of the bulk band structure further completes the picture by yielding field and Landau index-dependent masses.

IV. CONCLUSIONS AND SUMMARY

The present paper developed a self-consistent theory of electronic structure in the presence of strong magnetic fields for electrons in the space-charge layer of a III-V NGS MOSFET. The theory uses the effective-mass approximation and the multiband Kane Hamiltonian within the Hartree approximation. The interface between the insulator and the NGS is taken care of through adequately derived boundary conditions for the spinor wave function. These BC lead, as they ought, to a vanishing current[6] as the potential barrier in the insulator becomes infinitely high.

The computation of the energy levels proceeded in two stages. (1) In the first step the magnetic field **B** is set to zero and the self-consistent potential $V(x)$ [or $V(Z)$] is calculated. (2) In the second step we let $\mathbf{B}\neq 0$ and use $V(Z)$ in the Hamiltonian which we transform using a special rotation matrix and write in a way which makes the mathematical structure of the $\mathbf{B}=0$ case of stage (1) obvious. This has the advantage of making the computer codes of step (1) useful in step (2) as well; physically it also helps see more clearly the mechanisms which are at work in spin splitting the energy levels.

To make the theory more widely useful, we discuss it for three different models: the eight-band model, the six-band model, and the spinless four-band model and we derive appropriate BC for all three cases. Our self-consistent computations are carried out on InSb within the six-band model. In the absence of magnetic fields ($\mathbf{B}=0$) we compute several physical quantities such as the self-consistent potential $V(x)$, the subband structure, the electric-field-induced spin splitting of the subbands, the subband occupancies, the Fermi energy, and the subband density of state mass at the Fermi level. Our calculated subband occupancies show excellent agreement with the experimental data of other workers; however, the calculated subband density-of-state mass does not show such a good agreement. We used this result to discredit the use of $\mathbf{B}=0$ theories in $\mathbf{B}\neq 0$ experiments (e.g., CR) on NGS. To describe properly the experimental trends of the CR mass in NGS inversion layers, one has to include the effects of the **B** field because of the strong nonparabolicity of the Γ_6 bulk conduction band. The calculated $\mathbf{B}\neq 0$ energy levels show a fairly complex spectrum with LL of higher subbands merging with levels of lower ones due to the very small mass and the large g factor. The $\mathbf{B}\neq 0$ theory is aimed at interpreting experimental data; the values of **B**, at which the computation of the Landau ladder is performed, are taken directly from CR traces found in Ref. 4. Comparison between our calculated cyclotron resonance masses and experiment yields the following: (i) The $\mathbf{B}\neq 0$ CR masses are brought closer to the experimental ones as compared to their $\mathbf{B}=0$ counterparts, contrary to what was believed.[4] (ii) The CR masses show some structure as a function of $N_{\rm inv}$ which follows quite well the structure observed experimentally and which was absent from the $\mathbf{B}=0$ density-of-state masses. (iii) The structure in (ii) is attributed to the combination of two factors: (a) The dependence of the CR mass on the Landau and spin indices n and σ, respectively, because of nonparabolicity, and (b) oscillations of the Fermi energy $E_F(\mathbf{B}\neq 0)$ with respect to $E_F(\mathbf{B}=0)$ as $N_{\rm inv}$ is varied.

The present theory applied to InSb MOSFETS applies equally well to other systems, e.g., $Cd_{1-x}Hg_xTe$ and other III-V NGS. It can also be applied with minor modifications to CdTe/InSb heterojunctions and doped quantum wells.

ACKNOWLEDGMENTS

The author is very indebted to Professor L. J. Sham for helpful dicussions, and to the University of California, San Diego, Physics Department computer center where the calculations have been carried out in part. He also acknowledges financial support from the Algerian Ministry of Higher Education under Grants Nos. D1901/-/23/96 and D1901/-/04/98.

APPENDIX A

Let s be an eigenfunction of the crystal Hamiltonian at Γ_6, the conduction-band minimum, and let x, y, and z be the spatial part of the eigenfunctions at the Γ_7 and Γ_8, the top of the valence band. Note that s, x, y, and z are periodic functions which transform like atomic s, x, y, and z atomic wave functions under the action of the tetrahedral point group. Let $\uparrow$ denote a spin-up state and $\downarrow$ a spin-down state with respect to the z axis. The basis vectors $|1\rangle,|2\rangle,...,|8\rangle$ are then given by

$$|1\rangle=|is\uparrow\rangle,$$

$$|2\rangle=|is\downarrow\rangle,$$

$$|3\rangle=-|(x+iy)/\sqrt{2}\uparrow\rangle,$$

$$|4\rangle=-|(x+iy)/\sqrt{6}\downarrow\rangle+\sqrt{2/3}|z\uparrow\rangle,$$

$$|5\rangle=\sqrt{2/3}|z\downarrow\rangle+|(x-iy)/\sqrt{6}\uparrow\rangle,$$

$$|6\rangle=|(x-iy)/\sqrt{2}\downarrow\rangle,$$

$$|7\rangle=|(x+iy)/\sqrt{3}\downarrow\rangle+|z\uparrow\rangle/\sqrt{3},$$

$$|8\rangle=-|z\downarrow\rangle/\sqrt{3}+|(x-iy)/\sqrt{3}\uparrow\rangle. \tag{A1}$$

Now let $k_z=0$ in the Hamiltonian and denote k_y by k, then the states $\{|1\rangle,|3\rangle,|5\rangle,|8\rangle\}$ decouple from the states $\{|2\rangle,|4\rangle,|6\rangle,|7\rangle\}$. Let us now define two new basis sets $\{|\mathrm{I}\rangle,...,|\mathrm{IV}\rangle\}$ and $\{|\mathrm{I}'\rangle,...,|\mathrm{IV}'\rangle\}$ with $|\mathrm{I}\rangle=|1\rangle$, $|\mathrm{II}\rangle=|3\rangle$, $|\mathrm{III}\rangle=|5\rangle$, $|\mathrm{IV}\rangle=|8\rangle$, and $|\mathrm{I}'\rangle=|2\rangle$, $|\mathrm{II}'\rangle=-|6\rangle$, $|\mathrm{III}'\rangle=-|4\rangle$, and $|\mathrm{IV}'\rangle=|7\rangle$. With respect to these two decoupled sets the Hamiltonian reads $H'=H^{(u)}\oplus H^{(d)}$, where $H^{(u)}$ and $H^{(d)}$ are written on the unprimed and primed basis vectors, respectively, and $H^{(u)}$ is explicitly given by

$$H^{(u)}=\begin{pmatrix} \varepsilon_g/2+V(x) & \frac{P}{\sqrt{2}}\left(i\frac{\partial}{\partial x}-ik\right) & \frac{P}{\sqrt{6}}\left(-i\frac{\partial}{\partial x}-ik\right) & \frac{P}{\sqrt{3}}\left(-i\frac{\partial}{\partial x}-ik\right) \\ \frac{P}{\sqrt{2}}\left(i\frac{\partial}{\partial x}+ik\right) & -\varepsilon_g/2+V(x) & 0 & 0 \\ \frac{P}{\sqrt{6}}\left(-i\frac{\partial}{\partial x}+ik\right) & 0 & -\varepsilon_g/2+V(x) & 0 \\ \frac{P}{\sqrt{3}}\left(-i\frac{\partial}{\partial x}+ik\right) & 0 & 0 & -\varepsilon_g/2-\Delta+V(x) \end{pmatrix} \tag{A2}$$

and $H^{(d)}$ obtains from $H^{(u)}$ by substituting k by $-k$.

At the interface $x=0$, the components of the wave function satisfy the BC,

$$\varphi_1^{(u)}(0)=i\left(-\frac{\sqrt{3}}{2}\varphi_2^{(u)}(0)+\frac{1}{2}\varphi_3^{(u)}(0)+\frac{1}{\sqrt{2}}\varphi_4^{(u)}(0)\right) \tag{A3}$$

with a corresponding expression for the spin-down case.

APPENDIX B

When the Landau index $n=-1$, Eqs. (28) and (29) cease to be valid and the eigenvalue problem of Sec. III becomes

$$\bar{h}|\Psi\rangle=E|\Psi\rangle, \tag{B1}$$

where $\bar{h}$ is a 4×4 matrix operator given by

$$\overline{h}=\begin{pmatrix} \varepsilon_g/2+V(Z) & -i\sqrt{\frac{2}{3}}P\frac{\partial}{\partial Z} & \frac{P}{s} & i\frac{P}{\sqrt{3}}\frac{\partial}{\partial Z} \\ -i\sqrt{\frac{2}{3}}P\frac{\partial}{\partial Z} & -\varepsilon_g/2+V(Z) & 0 & 0 \\ P/s & 0 & -\varepsilon_g/2+V(Z) & 0 \\ i\frac{P}{\sqrt{3}}\frac{\partial}{\partial Z} & 0 & 0 & -\varepsilon_g/2-\Delta+V(Z) \end{pmatrix} \tag{B2}$$

with the basis vectors being $|2\rangle$, $|5\rangle$, $|6\rangle$, and $|8\rangle$, respectively, whose expressions are given in Appendix A. Now we write

$$\Psi=\frac{e^{ikX}}{\sqrt{L}}{}^t[\varphi_2(Z)\varphi_5(Z)\varphi_6(Z)\varphi_8(Z)], \tag{B3}$$

and we must find the bound states of Eq. (B1) subject to the BC,

$$i\sqrt{2}\varphi_2(0)=\varphi_8(0)-\sqrt{2}\varphi_5(0). \tag{B4}$$

The solution of Eq. (B1) is now easy since it is amenable to the $\mathbf{B}=0$ case with very slight modifications in the computer codes. In solving Eq. (B1) within the six-band model, we found it useful to write $\overline{h}$ as $\overline{h_0}+\overline{h_1}$ with

$$\overline{h_0}=\begin{pmatrix} \varepsilon_g/2+V(Z) & -i\frac{P}{\sqrt{3}}\left(\sqrt{2}\frac{\partial}{\partial Z}+\frac{1}{s}\right) & \frac{P}{s} \\ i\frac{P}{\sqrt{3}}\left(-\sqrt{2}\frac{\partial}{\partial Z}+\frac{1}{s}\right) & -\varepsilon_g/2+V(Z) & 0 \\ \frac{P}{s} & 0 & -\varepsilon_g/2+V(Z) \end{pmatrix} \tag{B5}$$

and

$$\overline{h_1}=\frac{P}{s\sqrt{3}}\begin{pmatrix} 0 & i & 0 \\ -i & 0 & 0 \\ 0 & 0 & 0 \end{pmatrix}. \tag{B6}$$

Now let $\langle r|\Psi_\nu^{(0)}\rangle={}^t[\varphi_{2,\nu}(Z)\varphi_{5,\nu}(Z)\varphi_{6,\nu}(Z)]e^{ikX}/\sqrt{L}$ be a solution of $\overline{h_0}|\psi_\nu^{(0)}\rangle=\varepsilon_\nu|\psi_\nu^{(0)}\rangle$ and write $|\Psi\rangle$ as

$$|\Psi\rangle=\sum_\nu C_\nu|\Psi_\nu^{(0)}\rangle. \tag{B7}$$

Then

$$(\varepsilon_\nu-E)C_\nu+\sum_{\nu'=0}^{\infty}\langle\Psi_\nu^{(0)}|\overline{h_1}|\Psi_{\nu'}^{(0)}\rangle C_{\nu'}=0, \tag{B8}$$

which is now very easy to solve. Note that ε_ν is exactly equal to the semiclassical energy of the state and can be obtained from Sec. II by making the substitution $k=-\sqrt{2}/s$; $\overline{h_1}$ in this case represents the quantum corrections to this semiclassical approximation.

[1] E. O. Kane, J. Phys. Chem. Solids **1**, 249 (1957).

[2] H. J. Jiménez-Gonzalez, R. L. Aggarwal, and G. Favrot, Phys. Rev. B **49**, 4571 (1994); M. H. Weiler, R. L. Aggarwal, and B. Lax, *ibid.* **17**, 3269 (1978); R. Ranvaud, H. R. Trebin, U. Rossler, and F. Pollak, *ibid.* **20**, 701 (1979); R. L. Bell, Phys. Rev. Lett. **9**, 52 (1962).

[3] E. Gornik, Physica B & C **127**, 95 (1984); E. Gornik, W. Muller, and F. Kohl, IEEE Trans. Microwave Theory Tech. **MTT-22**, 991 (1974).

[4] U. Merkt, M. Horst, T. Evelbauer, and J. P. Kotthaus, Phys. Rev. B **34**, 7234 (1986).

[5] T. Ando, A. B. Fowler, and F. Stern, Rev. Mod. Phys. **54**, 437 (1982).

[6] W. Zawadzki, S. Klahn, and U. Merkt, Phys. Rev. Lett. **55**, 983 (1985).

[7] G. E. Marques and L. J. Sham, Surf. Sci. **113**, 131 (1982); G. E. Marquez, Ph.D. thesis, University of California, San Diego, 1982.

[8] Saadi Lamari and L. J. Sham, Phys. Rev. B **38**, 9810 (1988); Surf. Sci. **196**, 551 (1988); Saadi Lamari, Ph.D. thesis, University of California, San Diego, 1991.

[9] Saadi Lamari, Phys. Lett. A **200**, 387 (1995).

[10] I. Nachev, Semicond. Sci. Technol. **3**, 29 (1988); F. Malcher, I. Nachev, A. Ziegler, and U. Rossler, Z. Phys. B **68**, 437 (1987); Y. Takada, K. Arai, N. Uchimura, and Y. Uemura, J. Phys. Soc. Jpn. **49**, 1851 (1980).

[11] F. Malcher, G. Lommer, and U. Rossler, *Proceedings of the 18th International Conference on the Physics of Semiconductors*, edited by O. Engström (World Scientific, Singapore, 1987).
[12] K. Shiina *et al.*, Appl. Phys. Lett. **52**, 1306 (1988); Y. D. Zheng *et al.*, *ibid.* **49**, 1187 (1986).
[13] Ch. Sikorski and U. Merkt, Phys. Rev. Lett. **62**, 2164 (1989); P. Junkert *et al.*, Phys. Rev. B **49**, 4794 (1994).
[14] J. M. Luttinger and W. Kohn, Phys. Rev. **97**, 869 (1955).
[15] W. Kohn and L. J. Sham, Phys. Rev. **140**, 1133 (1965).
[16] W. Brenig and H. Kasai, Z. Phys. B **54**, 101 (1984).
[17] Rudolf E. Langer, Phys. Rev. **51**, 669 (1937).
[18] N. N. Lebedev, *Special Functions And Their Applications* (Dover, New York, 1972).
[19] *Numerical Data and Functional Relationships in Science and Technology*, edited by O. Madelung, Landolt-Börnstein, New Series, Group III, Vol. 22, Pt. a (Springer, Berlin, 1987), p. 133.